Journal Pre-proof

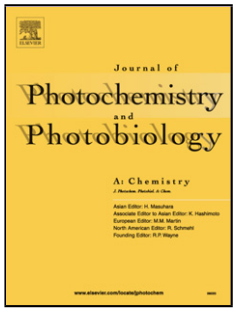

Graphitic Carbon Nitride for Efficient Fluorometric Quenching Bioassay of Hydrogen Peroxide: Effect of Structure on Properties

Aftab Ahmed (Conceptualization) (Writing - original draft), Akhtar Hayat (Conceptualization), Mian Hasnain Nawaz (Supervision), Peter John (Supervision) (Conceptualization), Muhammad Nasir

PII: S1010-6030(20)30530-X

DOI: https://doi.org/10.1016/j.jphotochem.2020.112731

Reference: JPC 112731

To appear in: *Journal of Photochemistry & Photobiology, A: Chemistry*

Received Date: 11 May 2020

Revised Date: 21 June 2020

Accepted Date: 26 June 2020

Please cite this article as: Ahmed A, Hayat A, Nawaz MH, John P, Nasir M, Graphitic Carbon Nitride for Efficient Fluorometric Quenching Bioassay of Hydrogen Peroxide: Effect of Structure on Properties, *Journal of Photochemistry and amp; Photobiology, A: Chemistry* (2020), doi: https://doi.org/10.1016/j.jphotochem.2020.112731

Graphitic Carbon Nitride for Efficient Fluorometric Quenching Bioassay of Hydrogen Peroxide: Effect of Structure on Properties

Aftab Ahmed[1, 2], Akhtar Hayat[1], Mian Hasnain Nawaz[1], Peter John[2*], Muhammad Nasir[1*]

[1] Interdisciplinary Research Centre in Biomedical Materials (IRCBM), COMSATS University Islamabad, Lahore Campus, 1.5 Km Defence Road, off Raiwind Road, Lahore, Punjab, Pakistan, 54000

[2] Government College University Lahore, Katchery Road, Anarkali, Lahore, Punjab, Pakistan 54000

Muhammad Nasir: Email; muhammadnasir@cuilahore.edu.pk, Tel; +92 (42) 111-001-007 Ext: 828, 829, Fax; +92 (42) 5321090

Peter John: Email; peterjohn@gcu.edu.pk, Tel; +92 (42) 111-000-010 Ext 262, +92 (42) 99213338

AUTHOR INFORMATION

Corresponding author

*Email: muhammadnasir@cuilahore.edu.pk (M. Nasir)

peterjohn@gcu.edu.pk (P. John)

ORCID iD

Muhammad Nasir: 0000-0002-6742-2721

Graphical Abstract:

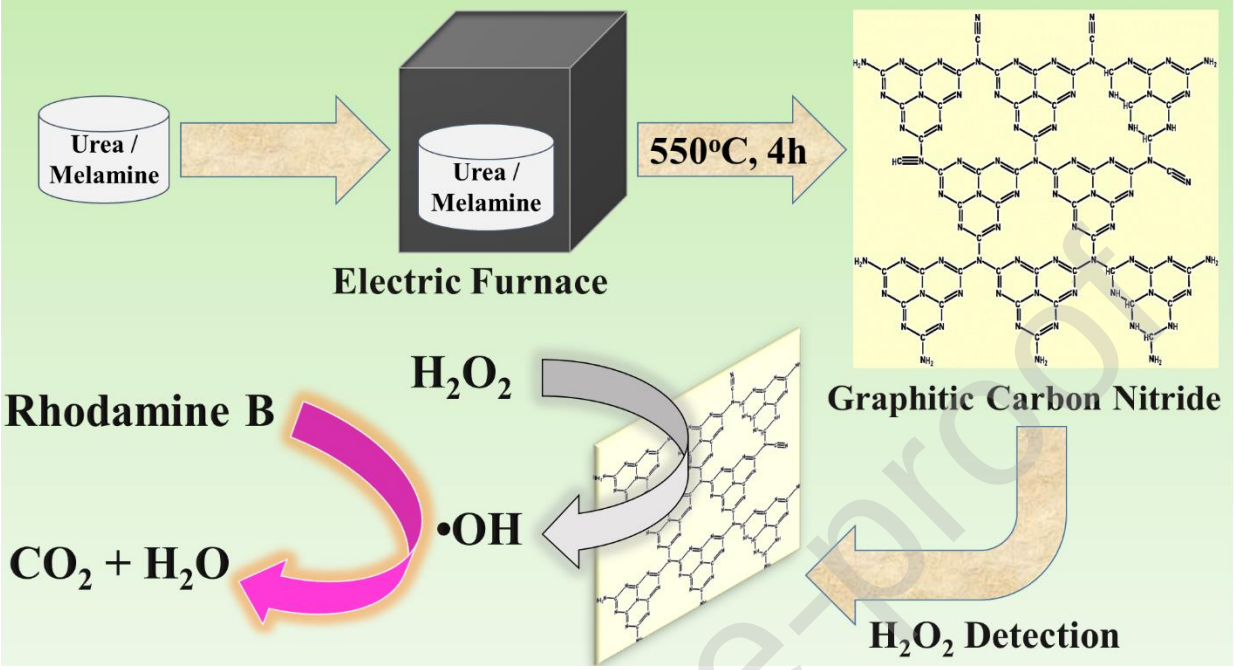

Schematic illustration of synthesis of Graphitic Carbon Nitride Nanosheets and procedure for fluorescence quenching based detection of H_2O_2 in the presence of RhB.

Highlights

- Effect of different precursors on the structure of graphitic carbon nitride was exploited in term of peroxidase-like-catalytic-activity by using fluorescence quenching of Rhodamine B to determine hydrogen peroxide
- Nanosheets of porous, folded along with curl edged fluffy g-C_3N_4 and crystalline smooth-surfaced planar g-C_3N_4 were prepared through liquid exfoliation ultrasonication method
- A possible reaction mechanism for the detection was proposed

- This method exhibited a linear range of 90 – 2500 nM and LOD of 73 nM.

ABSTRACT

Demand for sensitive and selective sensing of hydrogen peroxide is high because of its importance in various fields. So, metal-free nanostructures of g-C_3N_4 were synthesized and characterized through different techniques. Characterizations showed that g-C_3N_4 physicochemical properties were depended upon the nanostructure. A porous, thin and fluffy structure was got from urea, which possessed a much higher surface area and pore volume as compared to the planar and crystalline structured g-C_3N_4 got from melamine. A fluorescence quenching approach of hydrogen peroxide determination using catalyst nanosheets was used to explore the catalytic activity of these nanostructures. Because of the porosity, structural defects, smaller-crystallite size, and large surface area of the fluffy structured catalyst showed better quenching efficiency as compared to the flat and planar structured g-C_3N_4. An oxygen atom in urea played a role in changing the textural properties to porous and fluffy g-C_3N_4. Based on that, a selective, sensitive, and rapid sensing method was established having a wide linear range of 90 - 2500 nM, a lower detection limit of 73 nM, and a quantification limit of 220 nM.

KEYWORDS: Fluffy, Porous, Graphitic Carbon Nitride, Hydrogen Peroxide, Rhodamine B, Fluorescence Quenching.

1. INTRODUCTION

The H_2O_2 is generated in many physiological enzymatic catalytic processes. It has become a messenger of several abnormalities in the human body, such as oxidative stress, diabetes, renal failure, and cancer. [1] It is used in cosmetics and food industry, environmental protection, pharmaceutical, and clinical fields. This widespread use has made H_2O_2 determination very necessary. The H_2O_2 is diagnosed by reacting with natural-enzymes of horseradish-peroxidase [2] through colorimetric, electrochemical, [3] and luminescence techniques. [4] Despite high-selectivity of natural-enzymes, the detection process has faced the limitations of denaturing to environmental conditions, complicated and costly extraction and purification processes of the natural-enzymes. [5] To overcome these limitations, artificial enzyme-based sensors were designed and used in the assay of H_2O_2. Different artificial enzymes, such as Fe_3O_4 [6] nanoceria [7] and nitrogen-doped Titania [8] were reported for H_2O_2 bioassay.

Carbon-based nanomaterials are low-cost, less-toxic, and biocompatible. [9] Graphitic structured carbon-based nanomaterials like graphitic carbon nitride (g-C_3N_4) have reported as the catalyst in many analytical applications. It is used in fields such as photocatalytic production of hydrogen [10], degradation of organic pollutants [11, 12] pharmaceuticals and personal care products [13] and in the environmental remediation. The g-C_3N_4 has unique physicochemical properties, semiconductor behavior, and the □-conjugated network connecting two-dimensional layers of tris-s-triazine building blocks. It is fabricated and designed in different structures like nanoflowers, nanorods, and nanotube.

In this study, crystalline and porous g-C_3N_4 were synthesized from different precursors through the calcination method with no catalytic components or complex treatment to avoid toxicity. Characterization showed that porous and fluffy g-C_3N_4 have small-crystallite domain and structural-defects such as curling of nanosheets because of highly repeated graphitic-

structure as compared to crystalline and planar g-C_3N_4. Fluffy structure of g-C_3N_4 improved the optical properties and enhanced the surface area. Because of selectivity, high sensitivity, and handling of fluorescence quenching technique, a fluorescence quenching approach was explored using graphitic carbon nitride to build a detection assay of H_2O_2. The fluffy structure of g-C_3N_4 has shown better fluorescence quenching as compared to planar structured g-C_3N_4. The use of g-C_3N_4 in the present fluorescence quenching approach shortened the analysis time, lower limit of detection, formed broader linear range, and high sensitivity for H_2O_2 as compared to other methods of sensor development like colorimetric methods. Furthermore, the fluorescence quenching method was easier to use as the use of the colorimetric method. This study also helps in the high throughput synthesis of small-sized g-C_3N_4 nanosheets of the different nanostructures and investigating these nanosheets as peroxidase-like-mimics for biotechnology. [14] A summary of the synthesis process of catalyst and catalytic reaction mechanism between RhB and H_2O_2 are shown in Scheme 1.

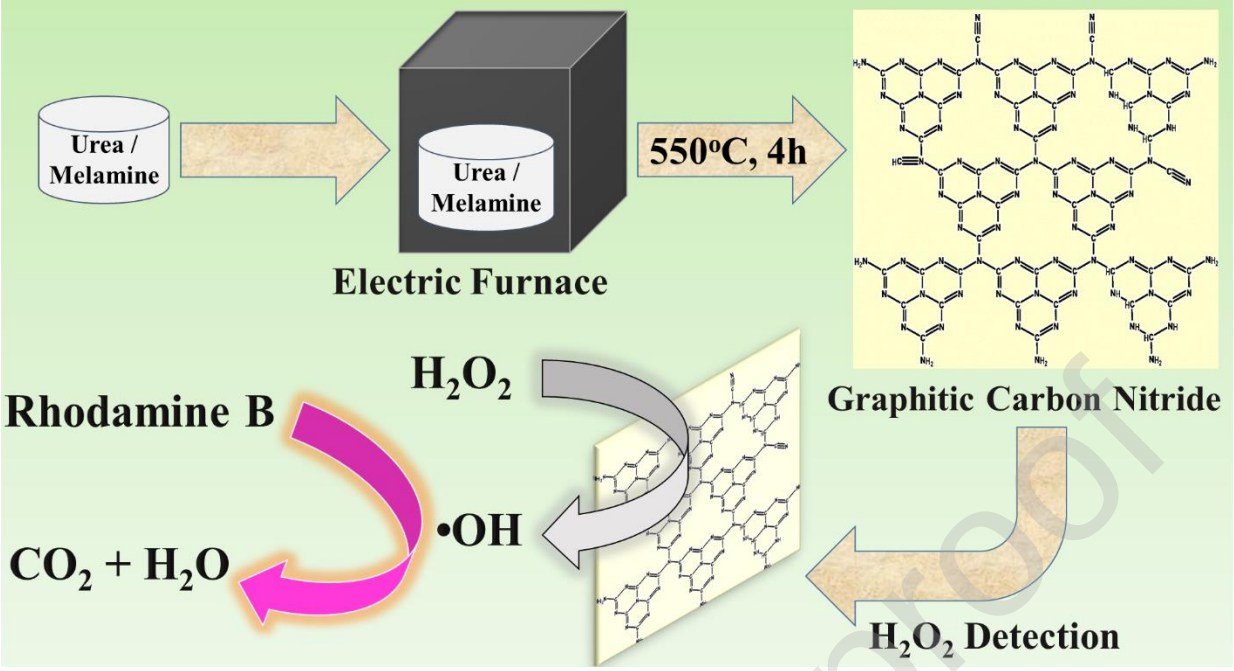

Scheme 1. Schematic illustration of calcination synthesis and reaction mechanism for H_2O_2 detection

2. EXPERIMENTATION

2.1 Materials and Reagents

Sodium acetate anhydrous, L (+)-ascorbic acid, and urea were received from Daejung. Melamine, citric acid, acetic acid, 3, 3′, 5, 5′-tetramethylbenzidine (TMB), and pyrocatechol were obtained from Sigma Aldrich. Rhodamine B was received from Avonchem. L-cysteine, p-benzoquinone (BQ), resorcinol, and H_2O_2 (30% of w/v solution) were obtained from Merck. Triethanolamine (TEOA), hydrochloric acid, D-glucose, tert-butyl alcohol (TBA), and uric acid were got from BDH chemicals Ltd. Dimethyl sulfoxide (DMSO) was obtained from Lab-Scan. Sodium hydroxide was got from Omicron. Phosphate buffer tablets (pH 7.2 ± 2, 10 mM) were received from VWR. PBS solution was prepared by dissolving PBS tablets in ultra-pure

deionized water of conductivity (<18 μΩ cm^{-1}), made in Elga Pure Ultra deionizer. All other reagents and chemicals were analytical-grade and used as got without further purification.

2.2 Apparatus

Scanning electron microscope images were got at 10 kV by using Vega 3 LMU Tescan SEM, attached with an energy dispersive spectrometer for EDX analysis. For SEM images and EDX analysis, samples were coated with a layer of gold, and coated samples were mounted on Aluminium support by using double adhesive tape. The adsorption isotherm data were used to measure the BET surface area (S_{BET}) by using a Tri-Star II (3020 2.00, USA) nitrogen gas adsorption apparatus. The pore size distribution was calculated via the Barret-Joyner-Halenda (BJH) method. XRD patterns were got with Rigaku D / max 2500 / PC XRD (Rigaku Corp Japan), equipped with a graphitic monochromator (40 kV, 40 mA). A nickel filtered copper-Kα radiation source (λ = 1.5418Å) was used during the sample analysis. Fourier transform infrared spectra were got from 660 – 4000 cm^{-1} on a Thermo Fisher Scientific FTIR spectrophotometer (Nicolet 6700). Ultraviolet-visible diffuse reflectance spectra were obtained on a Perkin Elmer Lambda 35 UV-Vis DRS spectrophotometer. UV-Vis absorption spectra were got on a Perkin Elmer Lambda 25 UV-Vis absorption spectrophotometer (UV - 25, Perkin Singapore). A bandwidth of 1 nm with a scan-rate of 960 nm min^{-1} was used for scanning absorption-spectra in the range from 400 - 800 nm. Photoluminescence spectra were scanned using a Reni Shaw PL-InVia-laser-scanning-confocal-microscope at a 457 nm excitation wavelength of the laser. Fluorescence measurements were performed on an Agilent Cary Eclipse fluorescence spectrophotometer.

2.3 Synthesis of g-C_3N_4

Differently, structured g-C_3N_4 was synthesized by a simple calcination method. For fluffy g-C_3N_4, 80 gram (g) of urea was grounded to a fine powder in a pestle mortar. Fine grounded urea powder was transferred to 100 mL ceramic crucible and covered the crucible with semi-closed ceramic lid. The urea was calcinated in the muffle-furnace with a temperature ramp of 5^oC min^{-1} up-to 550^oC and maintained this temperature for 4h. As-prepared product was washed with distilled water several times to remove any impurities and unreacted nitrogenous materials from the sample. The purified product was dried in an oven at 60^oC for 10h to get amorphous powder. The final dried product got from urea was labeled as PCN. Crystalline g-C_3N_4 got from melamine (10 g) as a precursor under the same synthesis protocol as PCN and labeled as CCN. Milky dispersion of exfoliated nanosheets containing 2.5 milligrams (mg) solid catalyst in one mL of the PBS was prepared via ultra-sonication at 25^oC for 15 min. These nanosheets-suspensions were stored at 4^oC in the refrigerator for further analysis.

2.4 Oxidation Reaction over PCN and CCN

Chromogenic substrates like terephthalaldehyde, [15] 2, 2′-azino-bis(3-ethylbenzothiazoline-6-sulfonic acid) diammonium salt, [16] and plasmonic-hot-electron transfer induced multicolor-chromogenic system [17] are reported for sensor development. TMB can act as peroxidase-substrate for the reaction with H_2O_2 in the presence of a catalyst. Oxidized-TMB showed the peroxidase-like activity of the catalyst in the reaction. So, an oxidation reaction between TMB and H_2O_2 was studied for determining our catalyst peroxidase-like activity. Typically, 40 μL of H_2O_2 solution (final concentration of 400 μM) was added to 1870 mL of sodium acetate buffer (pH = 5.0). Then, 60 μL of catalyst (PCN, CCN with a final concentration of 28 μg mL^{-1}) was added in the reaction mixture. The resultant reaction mixture was sonicated for 5 minutes. Finally, 30 μL of TMB solution (final concentrations of 50, 100, 200, 300, and

600 μM) was added to the reaction mixture at room temperature. The reaction color was changed to blue after a few seconds. The absorbance of the blue-color reaction mixture was monitored at 654 nm in 3 mL aliquots. Kinetic parameters were determined by using the Line-weaver-Burk plots of the double-reciprocal (1 / velocity against 1 / [substrate]) of Michaelis-Menten equation as follow

$$V = \frac{V_{maximal} \times [S]}{K_m + [S]}$$

Where $V_{maximal}$ was maximum reaction rate, V was initial velocity, K_m was Michaelis-Menten constant, and [S] was the concentration of the reacting-substrate.

2.5 Estimation of H_2O_2 by Fluorescence Methods

Chromogenic RhB can act as a fluorescence indicator for a reaction. In the present study, RhB was used as a fluorescence changing agent for varying catalytic activity of nanosheets in sensor development. Effect of reaction temperature, reaction time, pH, nanosheets concentration, and RhB dye concentration on sensor performance was also tested.

Fluorescence analysis was performed by incubating nanosheets and dye-containing reaction mixture with H_2O_2. For H_2O_2 detection, 28 μg mL^{-1} of nanosheets and 60 ng mL^{-1} of dye were mixed with different concentrations of H_2O_2 ($[H_2O_2]$) in 3 mL of the final volume. The $[H_2O_2]$ was varied in the range from 30 nM to 80000 nM. After incubation for one min at 24°C, reaction mixtures were added in 3 mL cuvette, and fluorescence emissions at 577 nm were recorded under an excitation wavelength of 554 nm. For fluorescence quenching of dye in nanosheets mixture by H_2O_2, change in fluorescence intensity at 577 nm was measured by using equation ($\Delta F_{577} = F_0 - F_{577}$). The F_0 and F_{577} nm showed the fluorescence emission

intensities of reaction mixtures containing dye and nanosheets in the absence and presence of H_2O_2 at 577 nm.

Other interferential experiments were performed under the same reaction conditions as above. For interferential-compound analysis, calcium chloride, potassium chloride, sodium chloride, glucose, resorcinol, uric acid, L-cysteine, ascorbic acid, dopamine, citric acid, and pyrocatechol were used in place of H_2O_2.

The mechanism of RhB oxidation was investigated by the addition of reactive-species scavengers in the reaction mixture. The main oxidative-species was detected by taking TEOA (5 mM) as hole-radical removal, TBA (10 mM) as an •OH radical scavenger, and BQ (5 mM) as a super-oxide scavenger in the reaction mixture.

3. RESULTS AND DISCUSSIONS

3.1 Characterizations

The nature of crystallization was found through XRD patterns. [18] XRD patterns of the prepared samples are displayed in **Fig. 1**. Both PCN and CCN have shown two diffraction peaks. PCN peak at 27.4^o gave a d-space of 0.324 nm, but the CCN peak gave a d-space of 0.34 nm. The PCN and CCN peaks at 27.4^o were indexed to (002) plane of inter-planar graphitic layer system (JCPDS 87-1526). This stacking-difference in the d-space of (002) peak of PCN and CCN represented a stranger binding between layers and more electron localization in PCN. PCN small-peak at 13.1^o with a d-spacing of 0.663 nm was indexed to (100) diffraction planes of the g-C_3N_4, which showed the stacking of the aromatic conjugated system (JCPDS 87-1526). Because of tilted angularity and structural defects, the d-spacing of the second (100) peak in PCN was smaller than that of the d-spacing of the tris-s-triazine unit of CCN as 0.713 nm. PCN

peaks were narrow and less-intense than CCN peaks, because of higher-polymerization, higher-porosity, smaller-crystalline domains, structural defects such as curling of nanosheets, and irregular repetition between graphitic layers. These factors could cause the higher catalytic activity of PCN. So, XRD spectra have confirmed a typical of g-C_3N_4 in PCN and CCN samples as reported by Wang et al. [19]

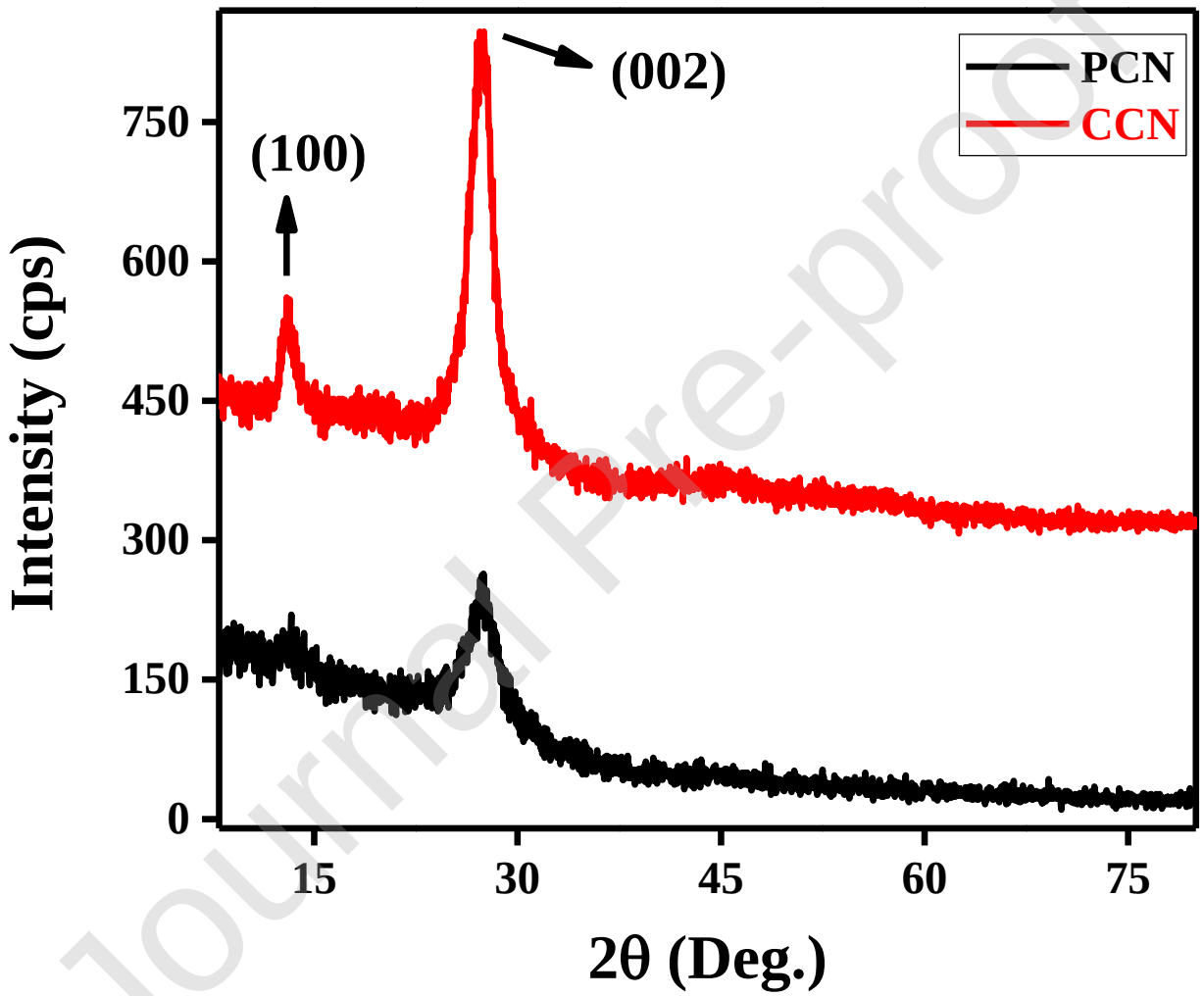

Fig. 1. XRD patterns of PCN and CCN

FTIR spectroscopy was used to detect the functional groups in the samples. [20] FTIR spectrum of PCN and CCN are displayed in Fig. 2. CCN spectrum showed peaks at 3099, 1620,

1536, 1397, 1313, 1229, 874 and 800 cm^{-1}. In contrast, the PCN spectrum showed a shift to higher wavenumber numbers for the peaks at 1627, 1558, 1410, 1320, and 1236 cm^{-1} as compared to corresponding CCN peaks. The higher shift in these PCN peaks positions may be attributed to the curled with porous structured nanosheets in PCN but planar with the crystalline structure in CCN. Broadband at 3099 cm^{-1} in the CCN spectrum and 3180 cm^{-1} in the PCN spectrum were assigned to stretching-vibrational modes of incompletely condensed NH_2 and NH bonds. This peak broadness may be attributed to water coordination with free N-H bonds. However, this peak shift to higher-wavenumber was assaigned to more uncondensed N-H bonds in PCN. Several bands in 1200 – 1700 cm^{-1} showed the characteristics of aromatic stretching modes of CN in aromatic heterocycle. The CCN peak at 1620 cm^{-1} and the PCN peak at 1627 cm^{-1} was assigned to NH bonds of the primary amine and C=N heterocycle. The higher shift of 22 cm^{-2} in the PCN peak (1558 cm^{-1}) as compared to CCN (1536 cm^{-1}) of stretching vibration of repeated units of triazine may be assigned to curling structure of nanosheets in PCN. The small band at 881 cm^{-1} for PCN and 874 cm^{-1} for CCN in the fingerprint region showed the out-of-plane C-H bonds in the aromatic domain. Peak around 800 cm^{-1} in CCN and 804 cm^{-1} in PCN spectra were corresponded to breathing vibrational modes of the s-triazine ring. All these findings have confirmed graphitic like structure in both PCN and CCN samples**.**

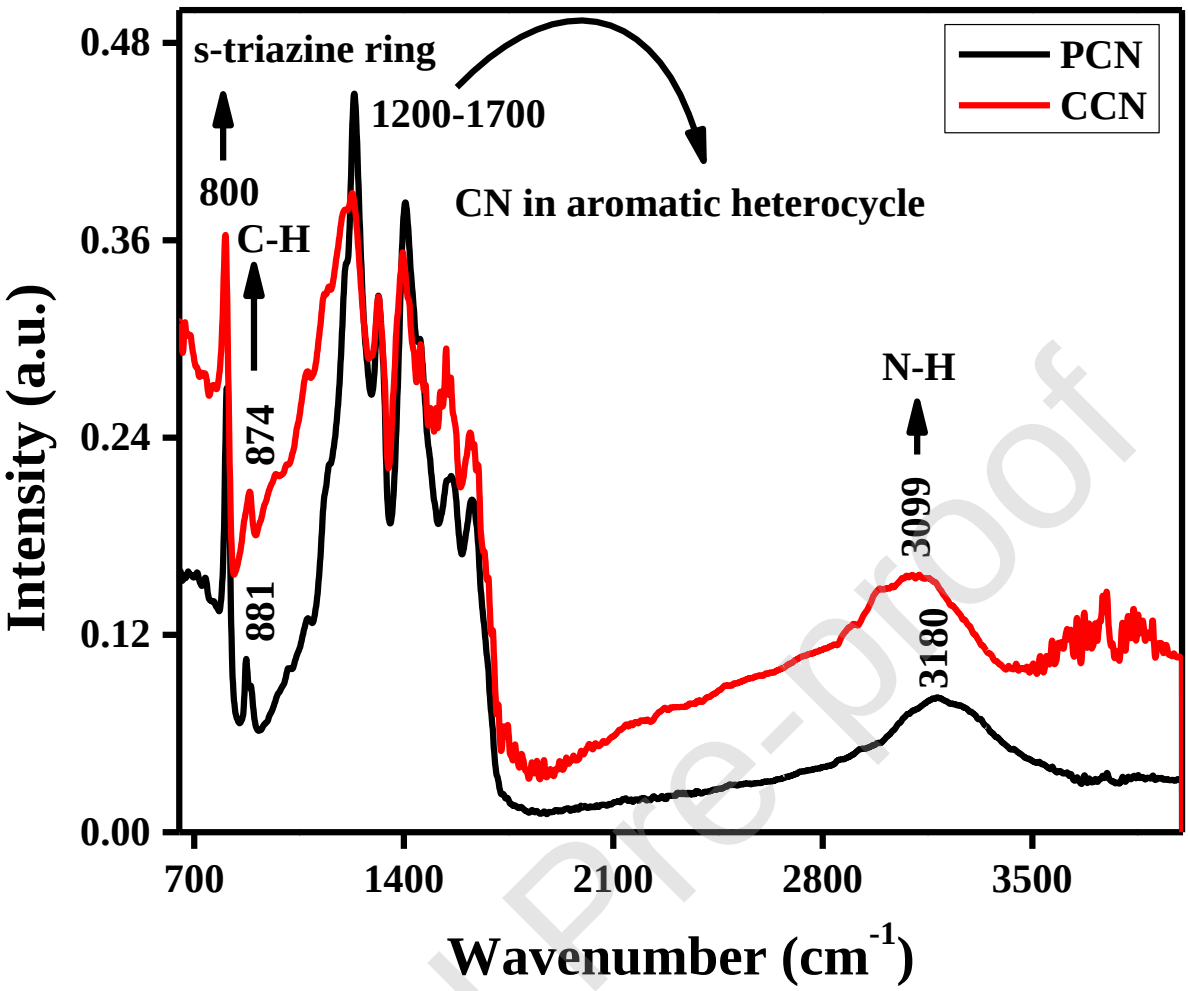

Fig. 2. FTIR spectrum of PCN and CCN

The effect of nanostructuring on optical properties like absorbance-edge and bandgap was determined by scanning UV-Vis DRS spectra of the samples, and resultant spectra are displayed in Fig. 3. All prepared samples have shown intrinsic semiconductors like absorption in the blue region of the visible light spectrum. Absorption edges for PCN and CCN were determined as 450 and 461 nm with corresponding band gaps of 2.75 and 2.69 eV using equation Eg = 1240/λ, [21] where Eg the bandgap and λ the absorption cut off of the semiconductor nanomaterials. Less-connected planar structure, the disorder in smaller crystalline domains, and

quantum confinement effect were considered as the main reasons for the higher bandgap of PCN as compared to CCN.

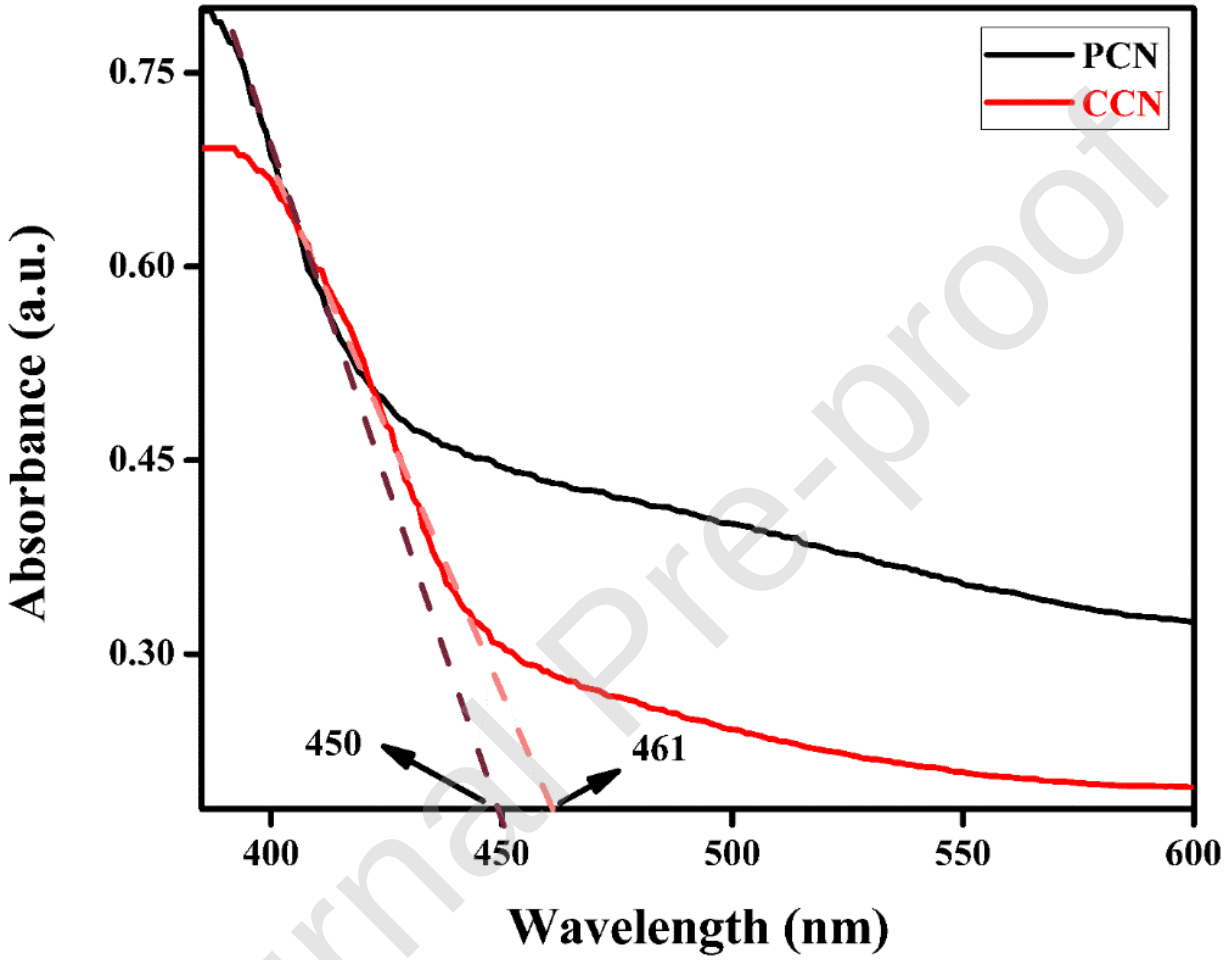

Fig. 3. UV-Vis DRS spectra of PCN and CCN

The texture and morphology of PCN and CCN were determined through the SEM. [22] The SEM images in Fig. 4 show the morphological and structural differences between PCN and CCN. PCN exhibited a fluffy-like structure with a small and irregular dense-texture as compared to CCN texture. These fluffy nanosheets were connected in such a way that they have left a small

hollow space between them. In comparison, CCN exhibited a uniform surface texture, and g-C_3N_4 crystalline sheets were looked like large-sized aggregates. A rocky and flowery surface of CCN was comprised of irregular flakes with an edge size of several nanometers. SEM images showed a structure in the prepared samples, which may be exfoliated to layers and nanosheets by ultra-sonication.

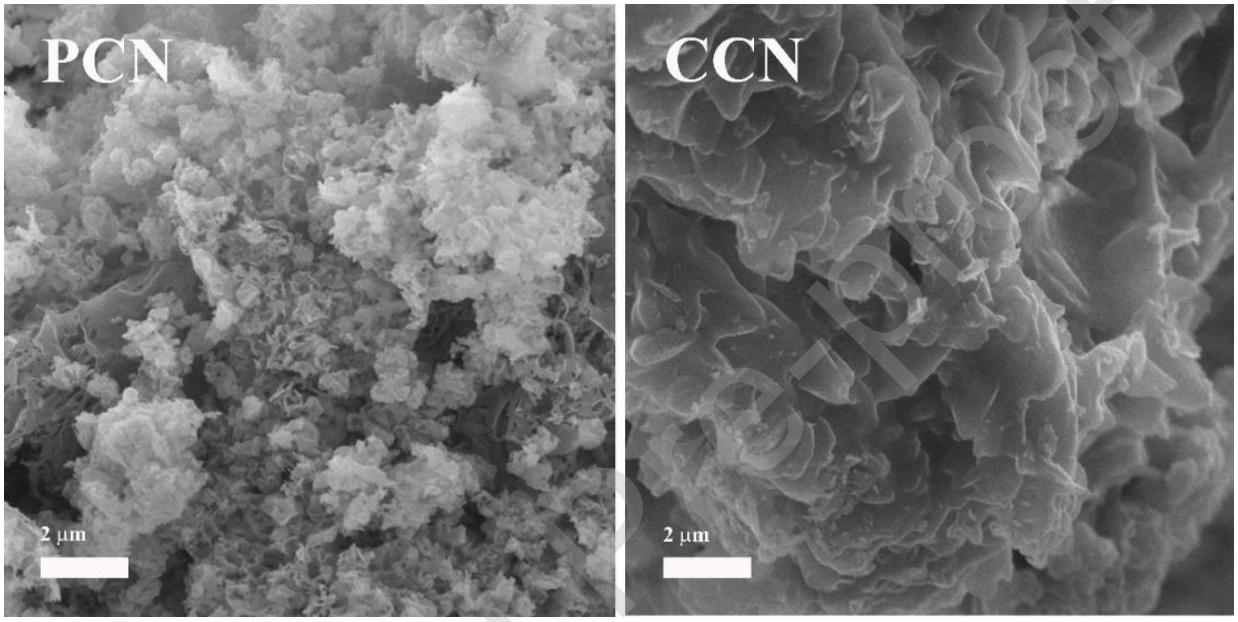

Fig. 4. SEM images of PCN and CCN

EDX analysis was used to find the purity and elemental composition of the samples. [23] EDX patterns of the PCN and CCN are displayed in Fig. 5. Carbon (C) and nitrogen (N) peaks in the EDX spectrum existed at their corresponding energy (KeV), which confirmed the g-C_3N_4 in both PCN and CCN. Except for C and N, no other elemental peak was observed in the spectrum of PCN and CCN, which showed that no impurities were present in synthesized samples.

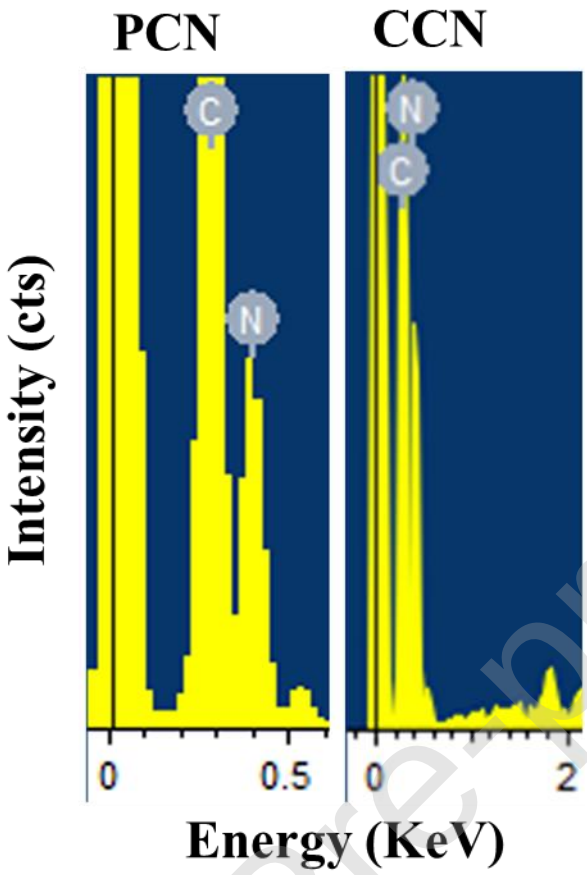

Fig. 5. EDX spectra of PCN and CCN

Table 1 shows the elemental composition in weight percentage (%) and the atomic percentage for PCN and CCN samples. C/N stoichiometric atomic ratio was calculated as 0.85 and 0.71 for PCN and CCN. The high deviation of the C/N ratio of PCN from the theoretical value of 0.75 has confirmed a non-perfect structure of the framework in PCN. Low C/N ratio of CCN from the theoretical C/N ratio of 0.75 can be related to the defects hindered charge separation and low charge transport property. [24]

Table 1. Weight (%) and atomic (%) of different elements present in the prepared samples

Sample	Elements	Weight (%)	Atomic (%)	C/N ratio (atomic)
PCN	C	41	45	0.85
	N	59	53	
CCN	C	36	40	0.71
	N	64	56	

The textural-properties, specific surface area, and pore size distribution of PCN and CCN were investigated by the nitrogen adsorption isotherm method. [25] Fig. 6 displays the nitrogen adsorption isotherm in the relative pressure (P/P_o) range of 0.01 - 1 for the prepared samples. Higher nitrogen adsorption of PCN as compared to that of the CCN showed the mesoporous morphology in PCN. Inset of Fig. 6 shows narrow pore-size-distribution curves of the as-prepared PCN and CCN samples in the mesoporous range from 20 to 200 Å. Large pores size of about 30 Å and 120 Å in the BJH pore-size-distribution curve of PCN has confirmed nanopores and mesopores in PCN.

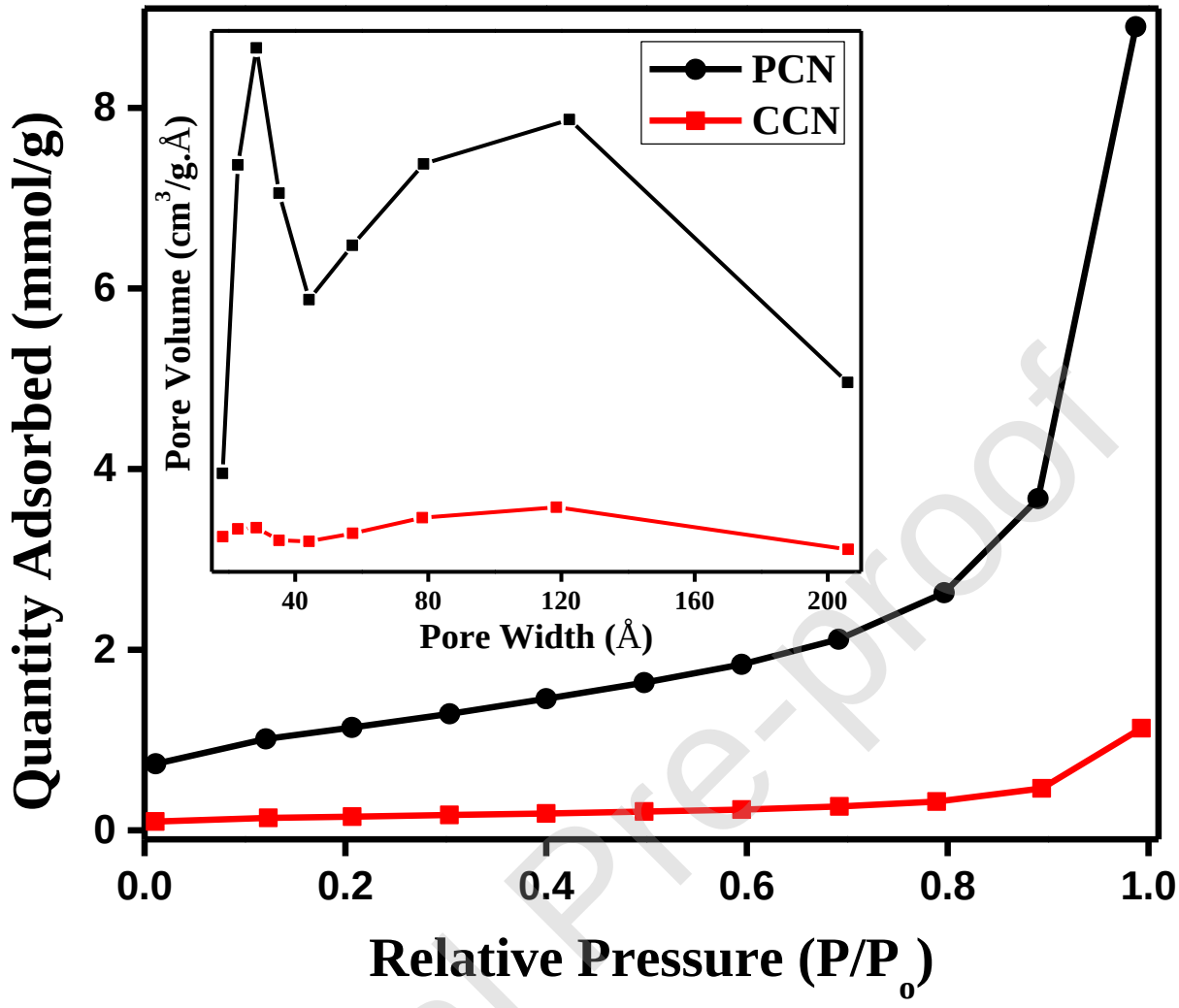

Fig. 6. Nitrogen adsorption isotherms (77K) and BHJ pore size distribution of PCN and CCN

A summary of the comparison of the specific surface area (S_{BET}), total pore volume, and pore width of PCN and CCN are listed in Table 2. PCN exhibited greater S_{BET} (89.9 m^2/g) than that of CCN (11.8 m^2/g). This enlarged surface area can be attributed to porous, thin, and curled nanosheets in fluffy PCN as compared to crystallized, planar, and large layered nanosheets of CCN. Urea was decomposed into more bubbles as compared to melamine during the thermal polymerization process, which can form the porous and fluffy structure in PCN. A larger surface area of the PCN showed that catalysts might offer more reactive sites for the reactions between

H_2O_2 and RhB, which can be expected to improve the catalytic activity of PCN. BJH adsorption volume of pores for PCN and CCN were calculated as 0.30 cm^3/g and 0.038 cm^3/g. The higher BJH adsorption cumulative volume of pores has confirmed porosity in PCN.

Table 2. The S_{BET} and pore properties of PCN and CCN

Samples	S_{BET} (m^2/g)	Pore Volume (cm^3/g)	Pore Width (Å)
PCN	89.9	0.3	146
CCN	11.8	0.038	178

Semiconductors have a high rate of electron-hole pair's recombination. Recombination rate and the effect of defects on the bandgap were determined through PL spectra. [26] PL spectra of the PCN and CCN samples are displayed in Fig. 7. PL emission peaks at the wavelengths (λ) of 604 and 570 nm for PCN and CCN can be attributed to electrons-holes pair's recombination. The difference in PL emission peak position represented variable sub-gaps defects distribution in both the samples. PCN peak intensity was smaller than CCN peak intensity because of the low recombination rate, and high separation of photo-induced electrons-holes pairs. These factors have confirmed the improved electron transferability of PCN, which was helpful in the sensing process.

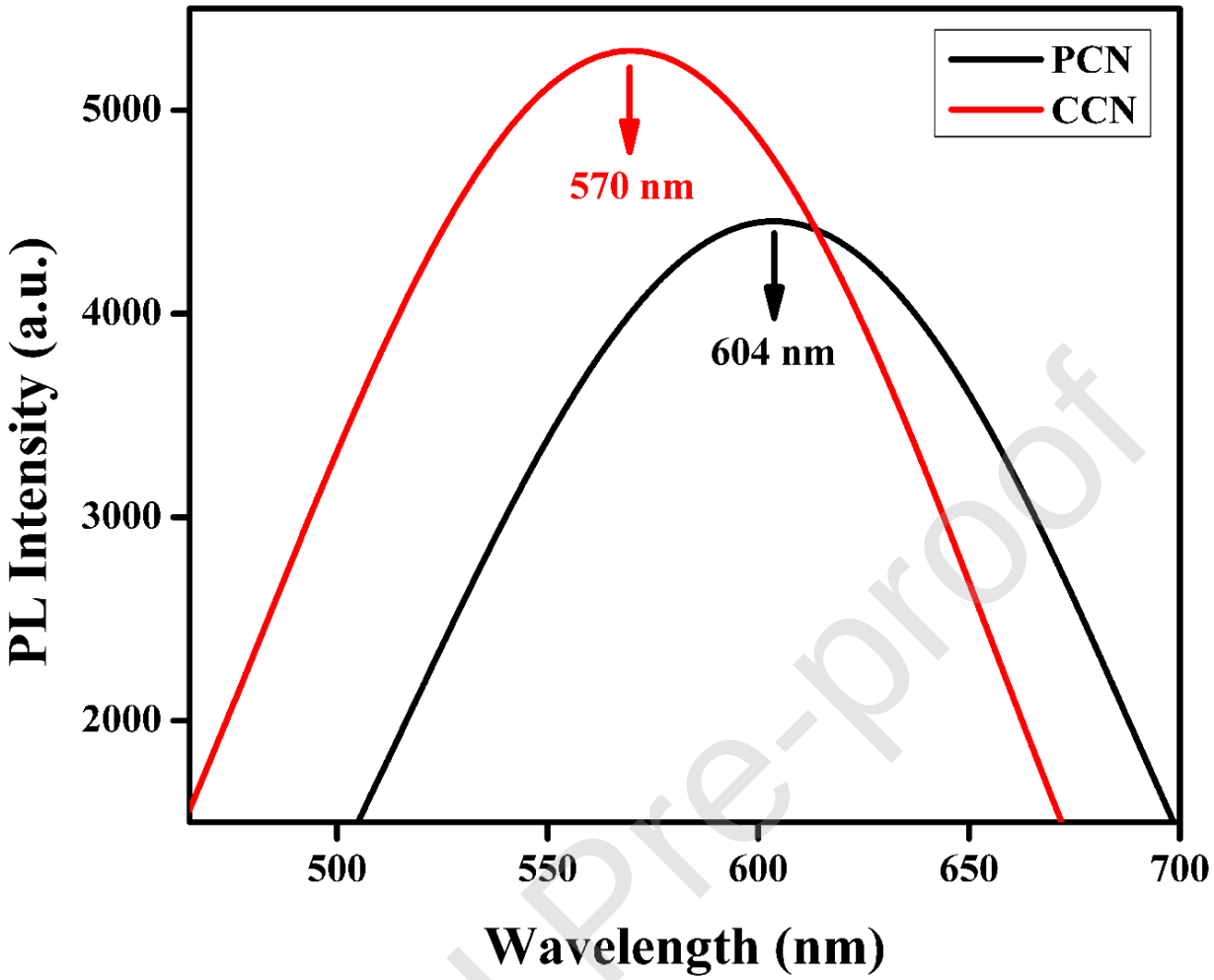

Fig. 7. PL spectra under an excitation wavelength of 457 nm

3.2 Catalytic Activity of the Nanosheets through Fluorescence Quenching Method

The activities of the as-prepared samples were investigated using catalytic-oxidation of RhB. The graphitic structure shows a useful electron transfer process through the graphitic-carbon network on the micro-level, [27] and such catalyst could reduce H_2O_2 by the donation and transfer of electrons. The activity of nanosheets was measured by the oxidation of RhB dye in H_2O_2 oxidant using the fluorescence quenching approach. Fig. 8A shows the pre-scan excitation and pre-scan emission spectra of RhB dye (60 ng mL^{-1}) in PBS (pH 7.2, 10 mM) solution at

room temperature. RhB solution exhibited an absorbance peak at 554 nm and an emission peak at 577 nm under an excitation of 340 nm. Fig. 8B shows that RhB under an excitation wavelength of 554 nm exhibited a fluorescence emission peak at 577 nm (curve a). This peak intensity was enhanced upon the H_2O_2 addition (curve b) in the reaction mixture because of the H_2O_2 chromophoric effect. Nanosheets and RhB incubation resulted in a dynamic equilibrium. RhB was adsorbed and aggregated onto the surface of the nanosheets, which decreased the fluorescence emission intensity (curves c and e) of the reaction mixture. H_2O_2 in reaction mixtures of RhB with nanosheets of PCN and CCN has reduced more emission intensities (curves d and f). This decreased intensity was because of a redox reaction between RhB and H_2O_2 under the catalytic influence. H_2O_2 was decomposed to radical and ions. Hydroxyl radical (•OH) was the main species [28] that oxidized chromogenic dye RhB to decrease its fluorescence intensity. [29] The decrease in fluorescence intensity of the reaction mixture containing PCN nanosheets (curve d) was higher than that of the reaction mixture containing CCN nanosheets (curve f). This emission difference can be attributed to the structure and morphology of PCN and CCN. Thin, porous, and fluffy with curled edged nanosheets of PCN have large surface areas, charge transportability, and more catalytic sites. Because of that, PCN nanosheets have shown better catalytic activity as compared to crystallized, flat, and planar CCN nanosheets. So, the sensor was designed using PCN nanosheets.

3.2 Mechanism of RhB Oxidation

Trapping experiments were performed by using different trapping-agents to determine the active-species during the oxidation process of RhB. TBA, TEOA, and BQ were added in the reaction mixtures to explore the oxidative species. Fig. 8C shows a comparison of the catalytic-activity of blank reaction-mixture with the catalytic-activities of different reaction-mixtures

containing TEOA, TBA, and BQ. Upon the addition of scavengers in the reaction-mixture of RhB, H_2O_2, and PCN, the catalytic-activity of the reaction-mixtures were suppressed. Trapped reactive-species can cause a decrease in catalytic-activities by suppressing RhB-oxidation. Most-lowering in ΔF_{577} nm was obtained for TBA containing reaction mixture, because of impairing of •OH. Relative-catalytic-activities of the TEOA reaction mixture were slightly decreased but not affected by BQ. These results showed that •OH radicals and holes were the active species for the reaction between RhB and H_2O_2 in the PCN catalyst.

Structural properties and high surface area of the PCN catalyst could improve the adsorption of H_2O_2, which could increase the dissociation of H_2O_2 to radicals. [30] Furthermore, due to energy transfer between the excited RhB and PCN catalyst, electron-hole pairs were created in the catalyst. These electron-holes pairs of PCN might activate the H_2O_2. The excited electron of the PCN may also reduce H_2O_2 to produce hydroxyl radicals. [30, 31] The proposed reaction mechanism of dye oxidation involved the generation of radicals. It can be expressed in equation form as follows:

$$\mathrm{RhB} + \text{Visible light} \rightarrow \mathrm{RhB}^{*}$$

$$\mathrm{RhB}^{*} + \mathrm{PCN} \rightarrow \mathrm{RhB} + \mathrm{PCN}\,(e^{-} + h^{+})$$

$$\mathrm{PCN}(e^{-}) + H_2O_2 \rightarrow OH^{\bullet} + OH^{-} + \mathrm{PCN}$$

$$\mathrm{PCN}(h^{+}) + H_2O \rightarrow OH^{\bullet} + H^{+} + \mathrm{PCN}$$

$$2H^{+} + 2OH^{-} \rightarrow 2H_2O$$

$$OH^{\bullet} + \mathrm{RhB} \rightarrow CO_2 + H_2$$

$$h^{+} + e^{-} \rightarrow (e^{-} + h^{+}) \text{ Negligible Recombination Reaction}$$

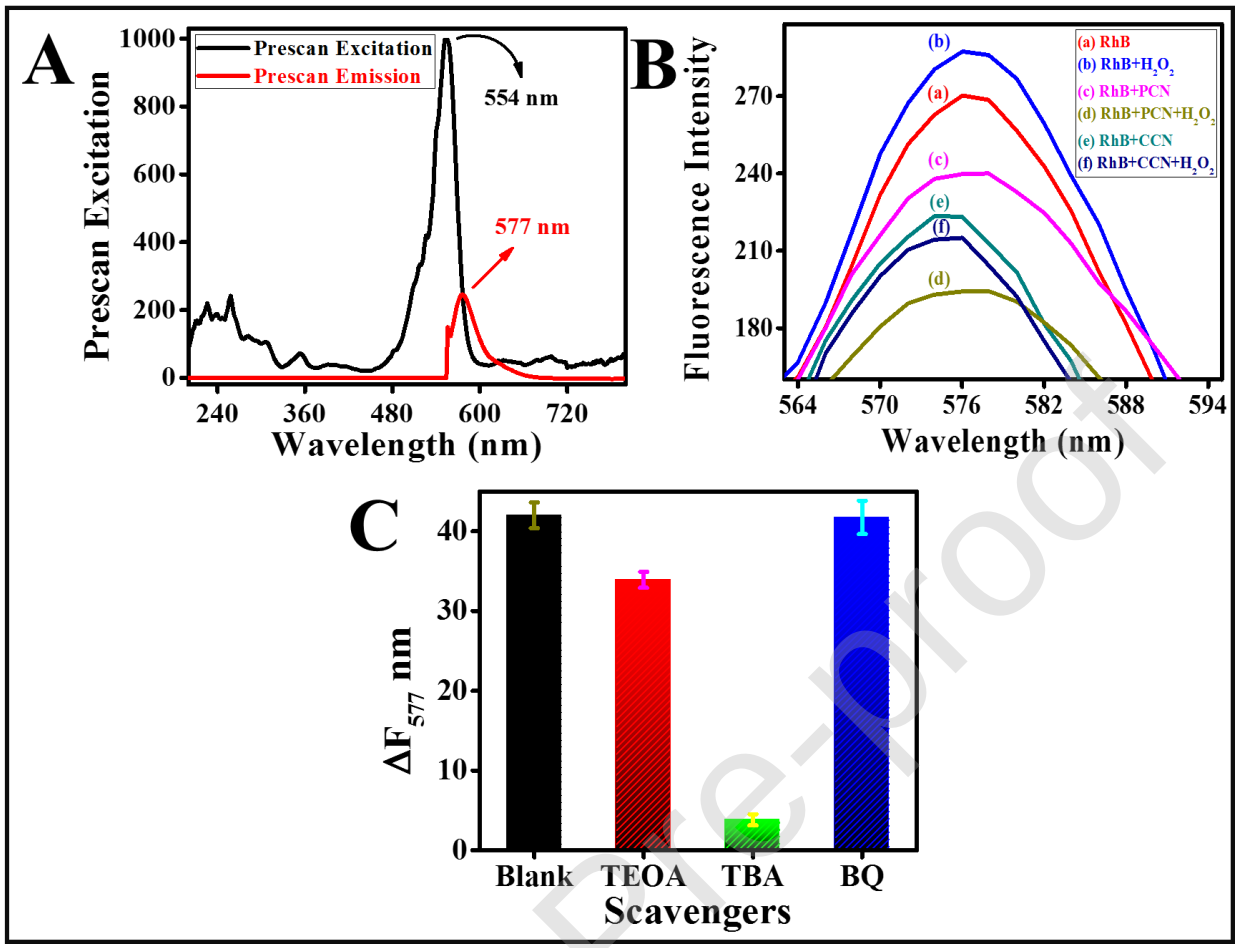

Fig. 8. Pre-scan of RhB under excitation at 340 nm (A), comparison of catalytic activity of PCN and CCN nanosheets (B), Effect of scavengers on the reactive species in the reaction (C). Reaction conditions were [RhB] = 60 ng mL^{-1}, [PCN] = 28 µg mL^{-1} and [H_2O_2] = 2500 nM in PBS (10 mM, pH 7.2) solution at room temperature.

3.3 Catalytic Activity of the Nanosheets through Colorimetric Method

The intrinsic-peroxidase-like activity of PCN was investigated by performing reactions at slightly acidic conditions of sodium acetate buffer (pH 5.0). Fig. 9A shows the high intrinsic peroxidase-like activity of PCN toward TMB oxidation in constant 400 µM of H_2O_2. Different control experiments without H_2O_2 or PCN showed no absorption peak and no activity toward

TMB oxidation (300 μM). The absorption intensity of the reaction mixture of PCN was higher than the CCN containing reaction mixture. The absorption intensity of PCN can be attributed to the structural, optical, and electronic properties of the catalyst. Inset of Fig. 9A shows the digital image of the blue color of the different reaction mixtures towards TMB oxidation after 1h of reaction. The reaction mixture of PCN has shown more-blue color as compared to the rest of the reaction mixture. This naked-eye observation also confirmed the higher peroxidase-like activity of PCN.

The optimum concentration of PCN nanosheets is determined from Fig. 9B. The optimal PCN amount was 28 μg mL^{-1}. Fig. 9C shows the relationship between the peroxidase-like activity of PCN and TMB substrate. PCN peroxidase-like activity was increased with TMB concentration. The steady-state kinetics was used to investigate the mechanism of PCN peroxidase-like-catalytic action with varied TMB concentrations at constant experimental conditions. Steady-state kinetics analysis showed that the PCN catalyst followed the typical Michaelis−Menten equation towards TMB oxidation. Different kinetics constants are determined towards TMB oxidation at pH of 5.0 and compared with Horseradish Peroxide (HRP) enzyme kinetics parameters in Table 3.

Table 3. Comparison of kinetics parameters of HRP with PCN towards TMB substrate

Catalyst	**K_m (mM)**	**V_{max}**	**Ref.**
PCN	0.159	1.3 (10^{-8} Ms^{-1})	**Present work**
HRP Enzyme	0.434	10 (10^{-8} Ms^{-1})	[32]

Michaelis-Menten constant (K_m) of HRP was 0.434 mM toward TMB substrate, which was higher than our PCN system parameters (0.159 mM). This K_m value of PCN catalyst may represent a strong affinity for TMB as compared to natural enzymes for TMB. **Fig. 9D** displays the reaction mechanism of TMB oxidation.

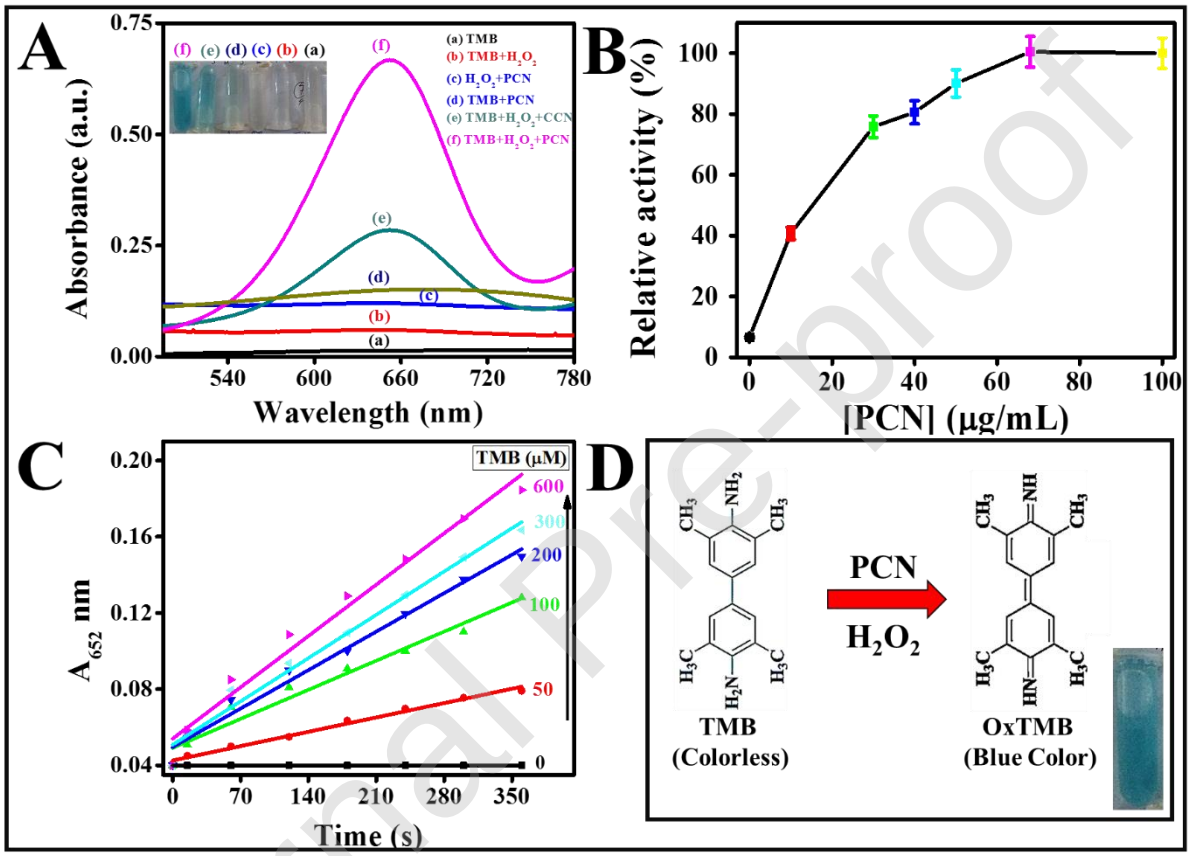

Fig. 9. Absorption spectra of reaction mixtures containing H_2O_2, TMB, and catalytic-nanomaterials in acetate-buffer solution (pH 5.0) after 1h of reaction time (A). Effect of PCN concentration (B) and TMB concentration on peroxidase-like activity (C). A mechanism for the reaction between TMB and H_2O_2 under the peroxidase-like PCN catalyst (D). Reaction conditions were [TMB] = 300 μM, [PCN] = 28 μg mL^{-1} and [H_2O_2] = 400 μM in sodium acetate buffer (10 mM, pH 5.0) solution at room temperature.

3.4 Optimization of Reaction Conditions

Fluorescence quenching of dye depends upon the reaction time, reaction temperature, pH, nanosheets concentrations, and dye concentrations. These reaction conditions are optimized for the development of an excellent sensor. [33] The ΔF_{577} nm represented the catalytic activity of PCN nanosheets. The influence of reaction conditions on ΔF_{577} nm was determined by taking $[H_2O_2]$ as 2500 nM in the reaction mixture.

Temperature and time effect on the catalytic-activity of PCN nanosheets between 5 – 70^oC and 0 – 30 min are displayed in Fig. 10A-10B. The greatest fluorescence quenching was observed if the reaction performed at 20^oC for one min. Thus, one min and 20^oC of reaction time and reaction temperature were adopted in this H_2O_2 assay. Hydrochloric acid and sodium hydroxide solutions were used to adjust the pH of the PBS solution. The pH was optimized between 3.0 – 10.0 and the effect of change in pH on ΔF_{577} nm are displayed in Fig. 10C. It is cleared from Fig. 10C that the fluorescence quenching of reaction mixture occurred in neutral and basic conditions. The ΔF_{577} nm was the greatest at pH of 8.0 because of the most and constant fluorescence quenching of the reaction system. So, 8.0 was the optimal value of pH, but later experiments were performed at neutral pH.

The efficiency of the assay is dependent upon the catalyst concentration. So, the optimal nanosheets concentration was determined to get better assay performance. Fluorescence quenching of reaction mixture was determined by increasing [PCN] nanosheets between 0 – 240 µg mL^{-1} and resultant graph are displayed in Fig. 10D. Higher [PCN] nanosheets resulted in the lowering of fluorescence quenching signals. A significant increase in fluorescence quenching was observed when [PCN] varied from 0 to 28 µg mL^{-1}. Beyond 28 µg mL^{-1} of [PCN], there was no significant change in the ΔF_{577} nm. These results showed that PCN could catalyze the reaction

between RhB and H_2O_2 systems. For the maximum quenching efficiency, 28 µg mL^{-1} of PCN was enough. This low concentration of catalyst could reduce the assay cost and could enhance its sensitivity. Thus, 28 µg mL^{-1} of PCN nanosheets was selected for the high fluorescence quenching efficiency of the RhB and H_2O_2 systems.

The amount of dye also affects the assay performance. Effect of [RhB] on fluorescence quenching of reaction-mixture was studied from 0 to 70 nM, and resultants graphs are displayed in Fig. 10E. A constant fluorescence quenching of reaction mixture was found at 60 ng mL^{-1} of [RhB]. At high [RhB], the catalytic activity of the catalyst was inhibited, which could result in a decrease in the ΔF_{577} nm. So, 60 ng mL^{-1} of [RhB] was recommended for getting a high sensitivity in this H_2O_2 assay.

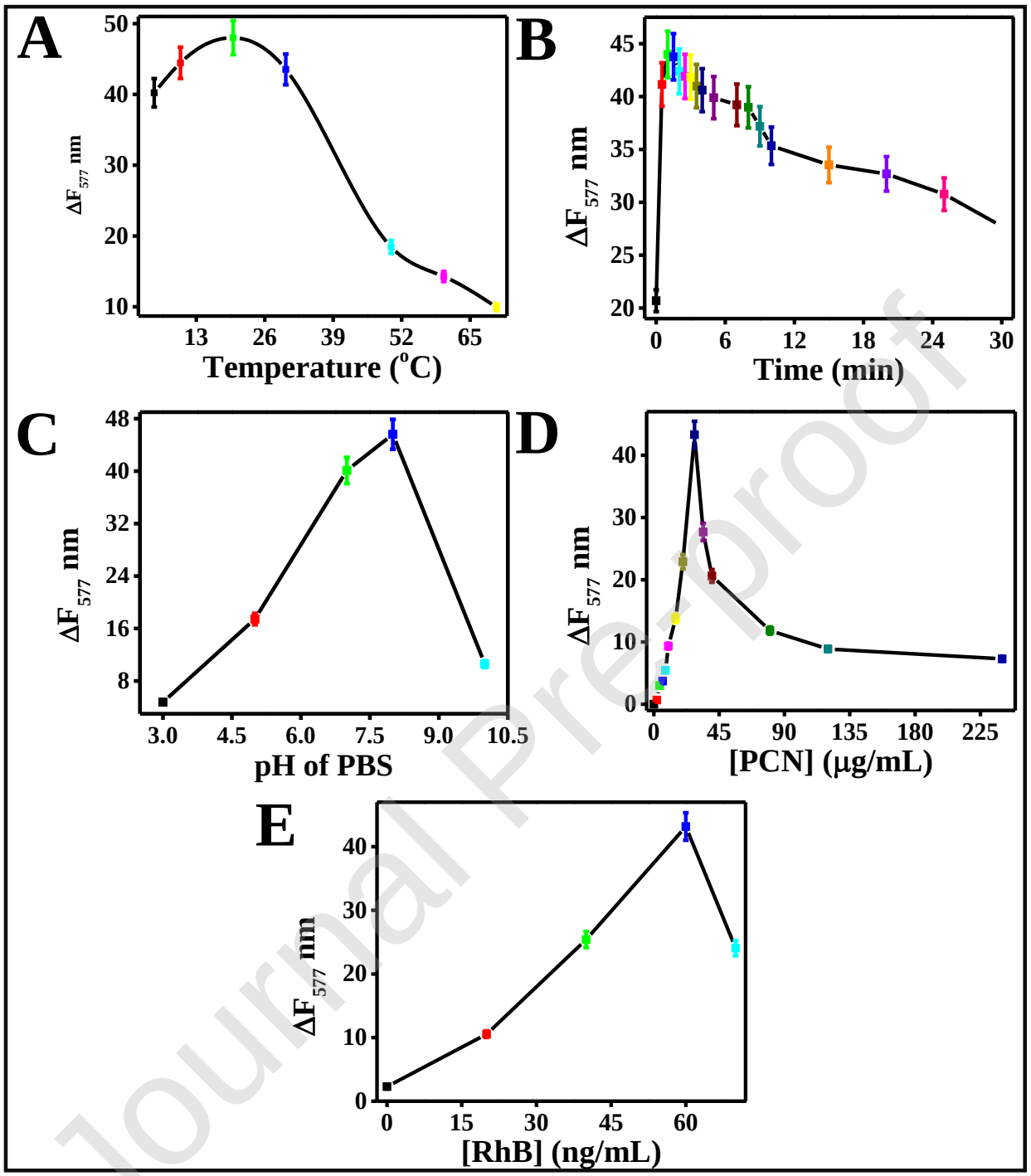

Fig. 10. Effect of temperature (A), time (B), pH (C), [PCN] (D), and [RhB] (E) on fluorescence quenching response under an excitation of 554 nm. Reaction conditions were the same as mentioned in Fig. 8.

3.5 H_2O_2 Detection using PCN Nanosheets

The influence of various [H_2O_2] on fluorescence quenching is required for developing the H_2O_2 assay. [34] The effect of various [H_2O_2] on fluorescence intensity of RhB and PCN nanosheets system in PBS solution under an excitation wavelength of 554 nm is displayed in Fig. 11A. Fluorescence intensity at 577 nm was decreased with an increase in [H_2O_2] from 0 to 2500 nM, reached to least intensity value, and then it was increased. The first decrease in fluorescence emission-intensity can be related to the oxidation of RhB molecules by first [H_2O_2]. However, the final increase in emission-intensity can be related to the hindrance in the catalytic-activity of PCN nanosheets at high [H_2O_2]. Quenching efficiency depends on transferring electrons and energy from PCN nanosheets to the quencher. A dose-response curve was required to find the relationship between ΔF_{577} nm and [H_2O_2]. The dose-response curve of the developing sensor in Fig. 11B shows that ΔF_{577} nm was varied with the change in [H_2O_2]. The ΔF_{577} nm was increased with increasing in [H_2O_2], and the maximum ΔF_{577} nm was observed at 2500 nM of [H_2O_2]. Thus, 2500 nM of [H_2O_2] was chosen as the best value from this experiment. A calibration curve was constructed at various [H_2O_2] by performing a series of reactions under the optimal reaction conditions, and resultants graphs are depicted in Fig. 11C. The graphical curve was linear from 90 to 2500 nM for H_2O_2 with a linear-fitting-regression equation ΔF_{577} nm $= 0.0167[H2O2] + 2.35512$ and a correlation coefficient (R^2) of 0.9923. The limit of detection ($LOD = 3\sigma/K$, where sigma (σ) was standard-error along Y-axis and K was the slope of linear-regression fitting curve) was calculated as 73 nM. Quantitation limit ($LOQ = 10\sigma/K$) was calculated as 220 nM.

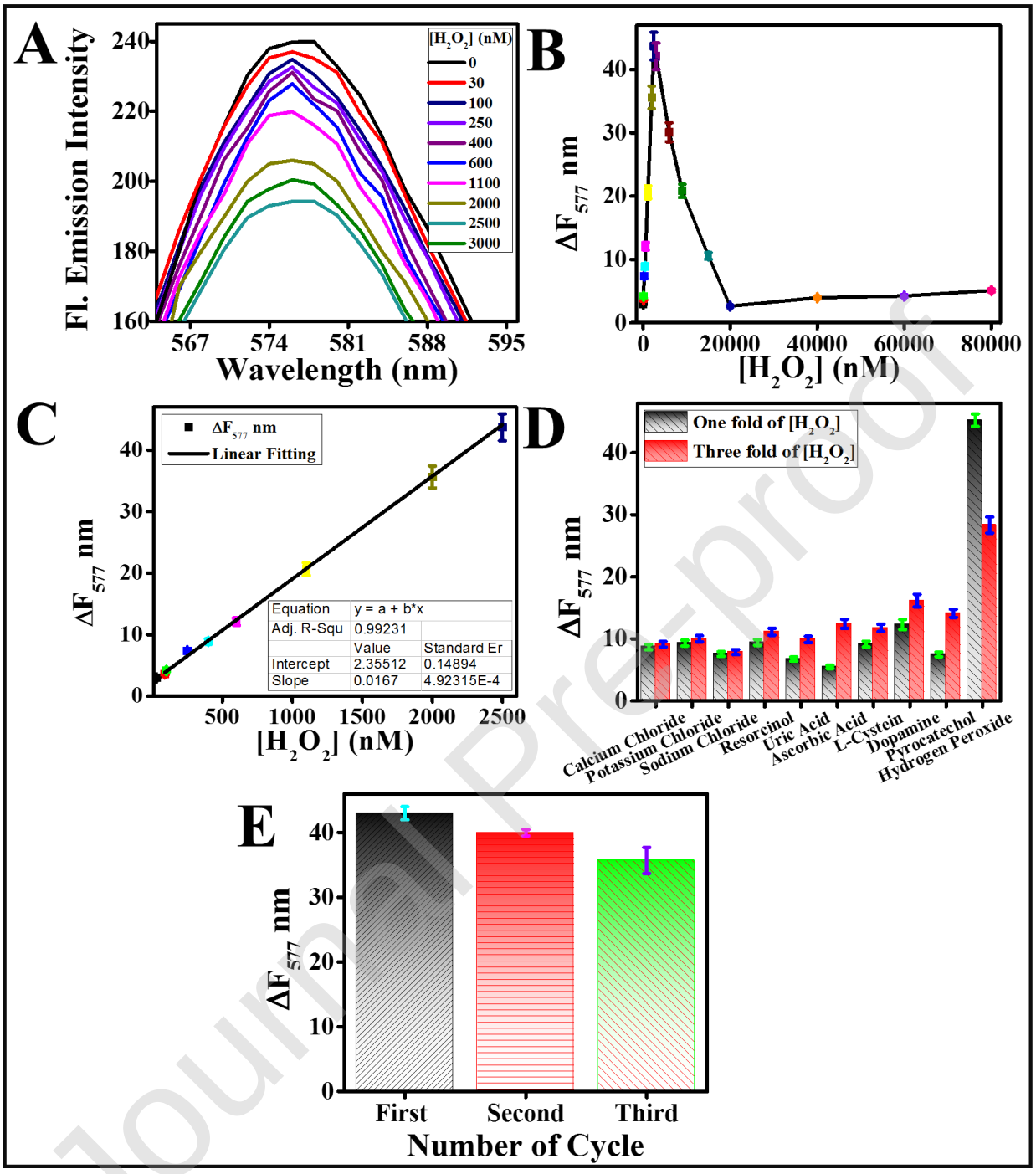

Fig. 11. Sensor response on various [H_2O_2] (0, 30, 100, 250, 400, 600, 1100, 2000, 2500 and 3000 nM) (A), dose-response curve (B), linear calibration curve (C), selectivity (D), and

recyclability (E) of the sensor for H_2O_2 determination. Reaction conditions were the same as detailed mentioned in Fig. 8.

Table 4. Comparison of different probes for H_2O_2 determination

Materials	Linear Range	LOD (nM)	Ref
PCN nanosheets	90 – 2500 nM	73	**Present work**
Glutathione-graphene quantum dots	0.5 – 10 μM	134	[35]
C-dots	0.5 – 100 μM	195	[36]
CdS/Ag_2S quantum dots	0.001 – 10 mM	300	[37]
Fe_3O_4 nanoparticles	10 – 200 nM	5.8	[34]
Polyethylene imine-capped Ag nanoclusters	0.5 – 100 μM	400	[38]
ZIF-8/Cu nanocomposites	10 – 1500 nM	10	[39]
Protonated g-C_3N_4	0.0016 – 3.72 mM	400	[40]

It is cleared from Table 4 that the sensitivity of our sensing platform was comparable or superior to other H_2O_2 sensing platforms. Our sensing system was metal-free and less-toxic than other reported systems. Hence, sensing-activity of PCN nanosheets in fluorescence quenching of RhB by H_2O_2 can be exploited as a probe.

3.6 The Selectivity of Sensor

The selectivity of the constructed sensor of RhB/PCN nanosheets was studied using different interfering materials in place of H_2O_2, and the resultants graph are displayed in Fig. 11D. The ΔF_{577} nm for H_2O_2 was remained the highest, when calcium chloride, potassium chloride, sodium chloride, resorcinol, uric acid, ascorbic acid, L-cysteine, dopamine, glucose,

citric acid, and pyro-catechol have the same concentration as H_2O_2 (2500 nM) and three times of [H_2O_2]. These findings showed that the developed sensor was selective for H_2O_2 over these species.

3.7 Recyclability of the Catalyst

The stability and recyclability of the PCN catalyst were significant for the oxidation-reaction of RhB with H_2O_2. The catalyst recycling tests were performed to find the effectiveness of PCN after several recycle-uses. PCN nanosheets were recovered from the first reaction by centrifuging the catalyst reaction-mixtures. Washed the PCN nanosheets with PBS solution and dried in the oven for 2h at 80^{o}C before reusing them in the next recycling-reactions. Fig. 11E shows a small-decrease in catalytic-activity of PCN even-after three reaction-cycles. The small-decrease in catalytic-activity was ascribed to loss of the catalyst during the recycling process. Such results showed that the PCN nanosheets could be reused again because of excellent stability.

4. CONCLUSION

In summary, nanostructures of g-C_3N_4 with semiconductor characteristics were synthesized by the calcination-method. The melamine and inexpensive, active oxygen-containing urea were used as precursors with no template. Detailed characterization revealed that prepared-nanostructures of g-C_3N_4 have different structural and physicochemical properties. Urea derived structure was fluffy, porous, and containing structural defects, smaller crystalline domains, and large surface area as compared to the melamine derived samples. Nanosheets were prepared through an ultrasonic-assisted exfoliation method for studying catalytic activity. Fluffy PCN has shown better experimental results as compared to CCN, because of this PCN was used as the

catalytic material in designing a fluorescence quenching probe for H_2O_2. PCN showed high activity because of a thin, porous, and curled fluffy nanosheets. The high sensitivity and selectivity of the PCN were significant. A linear relationship of the sensor was obtained between fluorescence quenching and H_2O_2 with the lower limit of detection as 73 nM. So, it was expected that this fluorescence quenching assay of H_2O_2 might allow researchers to design advanced g-C_3N_4 nanostructures and their use as a catalyst to improve or solve environmental-related problems.

Author Statement

Aftab Ahmed: Conceptualization, Experimentation, Characterization, Writing, Original draft preparation

Akhtar Hayat: Characterization, Writing, Conceptualization.

Mian Hasnain Nawaz: Characterization

Peter John: Supervision, Characterization

Muhammad Nasir: Supervision, Conceptualization, Characterization, Reviewing and Editing, Funding

Author Contributions

All authors have contributed and approved the final version of the manuscript.

Declaration of interests

The authors declare that they have no known competing financial interests or personal relationships that could have appeared to influence the work reported in this paper.

Funding Sources

This work supported by the Pakistan Science Foundation, Pakistan through its PSF-NSFC funded project (Project No. PSF/NSFC-II/Eng/P-COMSATS-Lhr (07)), and The World Academy of Sciences through COMSTECH-TWAS Joint Research Grants Programme having reference number 17-224 RG/MSN/AS_C – FR3240300073

Notes

The authors declare no competing financial interest.

ACKNOWLEDGMENT

Aftab Ahmed thanks Interdisciplinary Research Centre in Biomedical Materials (IRCBM), COMSATS University Islamabad, Lahore Campus to allow him to use its facilities and acknowledges the efforts of his seniors and colleagues in guiding him to complete his research work.

REFERENCES

[1] Y. Zhang, X. Bai, X. Wang, K.-K. Shiu, Y. Zhu, H. Jiang, Highly sensitive graphene–Pt nanocomposites amperometric biosensor and its application in living cell H2O2 detection, Analytical chemistry, 86 (2014) 9459-9465.

[2] T. Wang, H. Zhu, J. Zhuo, Z. Zhu, P. Papakonstantinou, G. Lubarsky, J. Lin, M. Li, Biosensor based on ultrasmall MoS2 nanoparticles for electrochemical detection of H2O2 released by cells at the nanomolar level, Analytical chemistry, 85 (2013) 10289-10295.

[3] L. Meng, D. Jiang, C. Xing, X. Lü, M. Chen, Synthesis and size-dependent electrochemical nonenzymatic H2O2 sensing of cuprous oxide nanocubes, RSC Advances, 5 (2015) 82496-82502.

[4] J.W. Liu, Y. Luo, Y.M. Wang, L.Y. Duan, J.H. Jiang, R.Q. Yu, Graphitic Carbon Nitride Nanosheets-Based Ratiometric Fluorescent Probe for Highly Sensitive Detection of H2O2 and Glucose, ACS applied materials & interfaces, 8 (2016) 33439-33445.

[5] Y. Tao, E. Ju, J. Ren, X. Qu, Bifunctionalized mesoporous silica-supported gold nanoparticles: intrinsic oxidase and peroxidase catalytic activities for antibacterial applications, Adv Mater, 27 (2015) 1097-1104.

[6] L. Gao, J. Zhuang, L. Nie, J. Zhang, Y. Zhang, N. Gu, T. Wang, J. Feng, D. Yang, S. Perrett, X. Yan, Intrinsic peroxidase-like activity of ferromagnetic nanoparticles, Nat Nanotechnol, 2 (2007) 577-583.

[7] A. Hayat, J. Cunningham, G. Bulbul, S. Andreescu, Evaluation of the oxidase like activity of nanoceria and its application in colorimetric assays, Anal Chim Acta, 885 (2015) 140-147.

[8] M. Nasir, S. Rauf, N. Muhammad, M. Hasnain Nawaz, A. Anwar Chaudhry, M. Hamza Malik, S. Ahmad Shahid, A. Hayat, Biomimetic nitrogen doped titania nanoparticles as a colorimetric platform for hydrogen peroxide detection, J Colloid Interface Sci, 505 (2017) 1147-1157.

[9] Z. Zhou, Y. Zhang, Y. Shen, S. Liu, Y. Zhang, Molecular engineering of polymeric carbon nitride: advancing applications from photocatalysis to biosensing and more, Chem Soc Rev, 47 (2018) 2298-2321.

[10] Y. Chen, Z. Zhan, J. Wang, Y. Shen, S. Liu, Y. Zhang, Solution-based processing of carbon nitride composite for boosted photocatalytic activities, Chinese Chemical Letters, 29 (2018) 437-440.

[11] T. Wang, C. Nie, Z. Ao, S. Wang, T. An, Recent progress in g-C3N4 quantum dots: synthesis, properties and applications in photocatalytic degradation of organic pollutants, Journal of Materials Chemistry A, 8 (2020) 485-502.
[12] M. Wu, X. He, B. Jing, T. Wang, C. Wang, Y. Qin, Z. Ao, S. Wang, T. An, Novel carbon and defects co-modified g-C3N4 for highly efficient photocatalytic degradation of bisphenol A under visible light, Journal of Hazardous Materials, 384 (2020) 121323.
[13] Y. Wang, B. Jing, F. Wang, S. Wang, X. Liu, Z. Ao, C. Li, Mechanism Insight into enhanced photodegradation of pharmaceuticals and personal care products in natural water matrix over crystalline graphitic carbon nitrides, Water Research, 180 (2020) 115925.
[14] J. Yu, X. Ma, W. Yin, Z. Gu, Synthesis of PVP-functionalized ultra-small MoS2 nanoparticles with intrinsic peroxidase-like activity for H2O2 and glucose detection, RSC Advances, 6 (2016) 81174-81183.
[15] R. Ai, Y. He, Covalent organic framework-inspired chromogenic system for visual colorimetric detection of carcinogenic 3, 3′-diaminobenzidine, Sensors and Actuators B: Chemical, 304 (2020) 127372.
[16] M. Zhao, J. Wang, H. Yu, Y. He, T. Duan, A highly selective and sensitive colorimetric assay for specific recognition element-free detection of uranyl ion, Sensors and Actuators B: Chemical, 307 (2020) 127664.
[17] J. Du, J. Wang, Y. Deng, Y. He, Plasmonic hot electron transfer-induced multicolor MoO3-x-based chromogenic system for visual and colorimetric determination of silver(I), Microchimica Acta, 187 (2020) 120.
[18] A. Thomas, A. Fischer, F. Goettmann, M. Antonietti, J.-O. Müller, R. Schlögl, J.M. Carlsson, Graphitic carbon nitride materials: variation of structure and morphology and their use as metal-free catalysts, Journal of Materials Chemistry, 18 (2008) 4893.
[19] X. Wang, K. Maeda, A. Thomas, K. Takanabe, G. Xin, J.M. Carlsson, K. Domen, M. Antonietti, A metal-free polymeric photocatalyst for hydrogen production from water under visible light, Nat Mater, 8 (2009) 76-80.
[20] S.C. Yan, Z.S. Li, Z.G. Zou, Photodegradation Performance of g-C3N4 Fabricated by Directly Heating Melamine, Langmuir, 25 (2009) 10397-10401.

[21] A.K.R. Police, S. Basavaraju, D.K. Valluri, S. Machiraju, J.S. Lee, CaFe2O4 sensitized hierarchical TiO2 photo composite for hydrogen production under solar light irradiation, Chemical engineering journal, 247 (2014) 152-160.
[22] Z.-A. Lan, G. Zhang, X. Wang, A facile synthesis of Br-modified g-C 3 N 4 semiconductors for photoredox water splitting, Applied Catalysis B: Environmental, 192 (2016) 116-125.
[23] G.P. Mane, D.S. Dhawale, C. Anand, K. Ariga, Q. Ji, M.A. Wahab, T. Mori, A. Vinu, Selective sensing performance of mesoporous carbon nitride with a highly ordered porous structure prepared from 3-amino-1,2,4-triazine, Journal of Materials Chemistry A, 1 (2013) 2913-2920.
[24] W.J. Ong, ; Tan, L. L.; Ng, Y. H.; Yong, S. T.; Chai, S. P.;, Graphitic Carbon Nitride (g‐C3N4)‐Based Photocatalysts for Artificial Photosynthesis and Environmental Remediation: Are We a Step Closer To Achieving Sustainability?, Chem. Rev., 116 (2016) 7159-7329.
[25] M. Zhang, J. Xu, R. Zong, Y. Zhu, Enhancement of visible light photocatalytic activities via porous structure of g-C3N4, Applied Catalysis B: Environmental, 147 (2014) 229-235.
[26] P. Wu, J. Wang, J. Zhao, L. Guo, F.E. Osterloh, Structure defects in g-C3N4 limit visible light driven hydrogen evolution and photovoltage, J. Mater. Chem. A, 2 (2014) 20338-20344.
[27] X. She, H. Xu, Y. Xu, J. Yan, J. Xia, L. Xu, Y. Song, Y. Jiang, Q. Zhang, H. Li, Exfoliated graphene-like carbon nitride in organic solvents: enhanced photocatalytic activity and highly selective and sensitive sensor for the detection of trace amounts of Cu2+, Journal of Materials Chemistry A, 2 (2014) 2563-2570.
[28] Z.-H. Diao, J.-J. Liu, Y.-X. Hu, L.-J. Kong, D. Jiang, X.-R. Xu, Comparative study of Rhodamine B degradation by the systems pyrite/H 2 O 2 and pyrite/persulfate: Reactivity, stability, products and mechanism, Separation and Purification Technology, 184 (2017) 374-383.
[29] Y. Cui, Z. Ding, P. Liu, M. Antonietti, X. Fu, X. Wang, Metal-free activation of H2O2 by g-C3N4 under visible light irradiation for the degradation of organic pollutants, Physical chemistry chemical physics : PCCP, 14 (2012) 1455-1462.
[30] T. Lin, L. Zhong, J. Wang, L. Guo, H. Wu, Q. Guo, F. Fu, G. Chen, Graphite-like carbon nitrides as peroxidase mimetics and their applications to glucose detection, Biosens Bioelectron, 59 (2014) 89-93.

[31] C. Zhou, X. Sun, J. Yan, B. Chen, P. Li, H. Wang, J. Liu, X. Dong, F. Xi, Thermo-driven catalytic degradation of organic dyes by graphitic carbon nitride with hydrogen peroxide, Powder Technology, 308 (2017) 114-122.
[32] W.P. Kwan, B.M. Voelker, Influence of Electrostatics on the Oxidation Rates of Organic Compounds in Heterogeneous Fenton Systems, Environmental Science & Technology, 38 (2004) 3425-3431.
[33] S. Srisantitham, M. Sukwattanasinitt, S. Unarunotai, Effect of pH on fluorescence quenching of organic dyes by graphene oxide, Colloids and Surfaces A: Physicochemical and Engineering Aspects, 550 (2018) 123-131.
[34] Z. Jiang, L. Kun, H. Ouyang, A. Liang, H. Jiang, A simple and sensitive fluorescence quenching method for the determination of H(2)O(2) using Rhodamine B and FE(3)O(4) nanocatalyst, J Fluoresc, 21 (2011) 2015-2020.
[35] Z. Qu, W. Na, Y. Nie, X. Su, A novel fluorimetric sensing strategy for highly sensitive detection of phytic acid and hydrogen peroxide, Anal Chim Acta, 1039 (2018) 74-81.
[36] N. Li, S.G. Liu, J.X. Dong, Y.Z. Fan, Y.J. Ju, H.Q. Luo, N.B. Li, Using high-energy phosphate as energy-donor and nucleus growth-inhibitor to prepare carbon dots for hydrogen peroxide related biosensing, Sensors and Actuators B: Chemical, 262 (2018) 780-788.
[37] L. Lin, Y. Wen, Y. Liang, N. Zhang, D. Xiao, Aqueous synthesis of Ag+doped CdS quantum dots and its application in H2O2sensing, Anal. Methods, 5 (2013) 457-464.
[38] T. Wen, F. Qu, N.B. Li, H.Q. Luo, Polyethyleneimine-capped silver nanoclusters as a fluorescence probe for sensitive detection of hydrogen peroxide and glucose, Anal Chim Acta, 749 (2012) 56-62.
[39] X. Hu, X. Liu, X. Zhang, H. Chai, Y. Huang, One-pot synthesis of the CuNCs/ZIF-8 nanocomposites for sensitively detecting H2O2 and screening of oxidase activity, Biosens Bioelectron, 105 (2018) 65-70.
[40] L. Liu, H. Lv, C. Wang, Z. Ao, G. Wang, Fabrication of the protonated graphitic carbon nitride nanosheets as enhanced electrochemical sensing platforms for hydrogen peroxide and paracetamol detection, Electrochimica Acta, 206 (2016) 259-269.